5G PPP

European Commission | Horizon 2020 European Union funding for Research & Innovation

5G-XHaul

Dynamically Reconfigurable Optical-Wireless Back-haul/Fronthaul with Cognitive Control Plane for Small Cells and Cloud-RANs

D4.2 Optical Fronthauling Solution

This project has received funding from the European Union's Framework Programme Horizon 2020 for research, technological development and demonstration

Advanced 5G Network Infrastructure for the Future Internet

Project Start Date: July 1st, 2015 Duration: 36 months

H2020-ICT-2014-2 671551 October 31st, 2017 – Version 1.0

Project co-funded by the European Commission

Under the H2020 programme

Dissemination Level: **Confidential**

Grant Agreement Number:	671551
Project Name:	Dynamically Reconfigurable Optical-Wireless Backhaul/Fronthaul with Cognitive Control Plane for Small Cells and Cloud-RANs
Project Acronym:	5G-XHaul
Document Number:	D4.2
Document Title:	Optical Fronthauling Solution
Version:	1.0
Delivery Date:	October 31st, 2017
Responsible:	ADVA Optical Networking SE (**ADVA**)
Editor(s):	Jim Zou (**ADVA**)
Authors:	Jim Zou (**ADVA**), Michael Eiselt (**ADVA**).
Keywords:	optical transport infrastructure, passive optical networks, wavelength division multiplexing, front-haul, WDM-PON, tuneable laser.
Status:	Final
Dissemination Level	Confidential
Project URL:	http://www.5g-xhaul-project.eu/

Version History

Rev. N	Description	Author	Date
0.1	First draft with ToC	Jim Zou (**ADVA**)	25/09/2017
0.2	Completed content	Jim Zou (**ADVA**)	26/10/2017
0.3	Draft for review	Jim Zou (**ADVA**)	30/10/2017
0.4	Formatting revision	Jesús Gutiérrez (**IHP**)	31/10/2017
1.0	Version for submission	Jesús Gutiérrez (**IHP**)	31/10/2017

Table of Contents

EXECUTIVE SUMMARY **8**

1. INTRODUCTION **9**

2. OVERVIEW OF FRONTHAUL IN 5G-XHAUL DATA PLANE **10**

2.1 Flexible Fronthaul Architecture **10**

2.2 System Concept with Remote Wavelength Control **11**

3. OPTICAL TRANSCEIVERS FOR FRONTHAUL **13**

3.1 Tuneable Laser Requirements **13**
3.1.1 Low Cost 13
3.1.2 Stability over Time 13
3.1.3 Simple Tuning Mechanism 13
3.1.4 Tuning Range 13

3.2 Available Laser Technologies **14**
3.2.1 Distributed Bragg Reflection (DBR) Lasers 14
3.2.2 Micro-Electromechanical System Vertical Cavity Surface Emitting Laser (MEMS-VCSEL) 14

3.3 Future Developments **15**

4. ENABLING TECHNOLOGY: PASSIVE WAVELENGTH-AGNOSTIC WDM **16**

4.1 Downstream Analysis **16**
4.1.1 AMCC Requirements 16
4.1.2 AMCC Performance 16
4.1.3 AMCC Impact on Payload 18

4.2 Upstream Analysis **18**
4.2.1 Pilot Tone Generation 19
4.2.2 Pilot Tone Impact on Data – Simulation 19
4.2.3 Pilot Tone Impact on Data – Measurements 20
4.2.4 Pilot Tone in Amplified System 21

4.3 Channel Crosstalk during Tuning **22**
4.3.1 Worst-Case Crosstalk Scenario 23
4.3.2 Experimental Crosstalk Analysis 23

5. SINGLE-WAVELENGTH CAPACITY OF 25G AND BEYOND **25**

5.1 DMT Modulation with PT **25**

5.2 Upstream Measurement Setup **25**

5.3 Results and Discussion **26**

6. CONCLUSIONS 29

7. REFERENCES 30

8. ACRONYMS 32

List of Figures

Figure 1: Overview of the WDM-PON-based FH link in the 5G-XHaul project. 10

Figure 2: WDM-PON system architecture flexibly connecting RRHs with BBUs. 10

Figure 3: Initial wavelength tuning based on the feedback of received power. 11

Figure 4: Wideband-tuneable semiconductor laser types (a) 5-section DS-DBR laser; (b) Sampled-Grating Y-branch laser. 14

Figure 5: (a) Cross section description of MEMS-VCSEL; (b) Photo of packaged LC-TOSA. 15

Figure 6: Measurement setup for AMCC sensitivity evaluation under the influence of the payload and vice versa. The eye-diagram inset shows a 2.5 Gbps payload signal with a 100 kbps NRZ envelope modulation. 17

Figure 7: BER vs. received power of an envelope modulated 100 kbps message channel. The modulation depth is varied from 7% to 11%. 17

Figure 8: Error floor as function of the modulation depth at -35 dBm for 100 kbps NRZ encoding compared to 50 kbps and 100 kbps Manchester encoding. 18

Figure 9: Bit error rate of the 2.5 Gbps payload channel vs. received power with (a) 10% and (b) 15% modulation depths of the envelope modulation. “No AMCC” is the case without envelope modulation. . 18

Figure 10: Pilot tone generation: (a) Adding a small sinusoidal current to the laser’s bias current; (b) dithering the bias voltage of external modulator. 19

Figure 11: Time-resolved PT modulation of mark P1(t) (black) and space P0(t) (grey).Upper row: multiplicative modulation; bottom row: additive modulation. Left column: PT frequency below lower cut-off frequency $f_{g,HP}$ (decision threshold (dashed) follows average power); right column: PT frequency above lower cut-off frequency $f_{g,HP}$ (decision threshold is constant). 20

Figure 12: Power penalty of data signal at BER of 10^{-9} as function of the extinction. (a) Multiplicative PT modulation; (b) additive PT modulation (circle and square curve overlay) (*m*: PT modulation depth; $f_{g,HP}$: Rx lower cut-off frequency). 20

Figure 13: Measurement setup for power penalty evaluation of a PT on a data signal in the case of multiplicative PT modulation scheme. 21

Figure 14: Measured power penalty of data signal as function of the PT frequency for different modulation depths. Left: 2.5 Gbps; right: 10 Gbps. (*m*: PT modulation depth). 21

Figure 15: EDFA impact on pilot tone (a) modulation-depth change Δm; (b) XGM. 22

Figure 16: Filter function of two cascaded 100 GHz spacing AWGs. Solid line: Target channel (A2→B2); dotted and dashed lines: crosstalk, when laser is connected to upper and lower neighbouring port of multiplexer filter (A1→B2 or A3→B2). 22

Figure 17: Setup for coherent and incoherent crosstalk evaluation with and without PT modulation. 23

Figure 18: Penalty measurement (a) incoherent crosstalk (Δ*f* ~50 GHz); (b) coherent crosstalk (Δ*f* ~0 GHz) without PT modulation. 24

Figure 19: Experimental setup for 26 Gbps DMT transmission up to 40 km SSMF transmission. 25

Figure 20: (a) Estimated SNR after 0 km SSMF for 3 measured wavelengths. (b) Estimated SNR after 40 km SSMF for 3 measured wavelengths. (c) Bit loading for 1530 nm wavelength after 0 km SSMF. (d) Bit loading for 1530 nm wavelength after 40 km SSMF. 27

Figure 21: BER vs. received power at 26 Gbps for different wavelengths and transmission reaches. 27

Figure 22: BER vs. transmission data rate for different wavelengths up to 20 km reach. 28

List of Tables

Table 1: Mean times between dropped and erred messages. 16
Table 2: DMT parameter overview. 25

Executive Summary

One of the objectives in Work Package 4 is to design and develop a flexible optical fronthaul solution supporting traffic aggregation and efficient coordination between the RRH and the BBU pool. Particularly, in the context of 5G-XHaul, we propose the use of WDM-PON technologies to support the fronthauling requirements of the 5G cloud radio access network (C-RAN) solution in the subtask 4.1.2.

Over the past few years, WDM-PONs have been proven to be a suitable and cost-effective solution in C-RAN environments to interconnect RRHs and BBUs, thanks to the bandwidth level it offers and its low deployment costs. This work involves the development of flexible broadband, high-bitrate per channel WDM-PONs that can serve the fronthaul on demand. This primarily relates to the bitrate of 10 Gbps today, with a potential path to higher bitrates in the near future. It should be noted that the optical fronthauling technologies will work in a complementary and coordinated fashion with the alternative mm-wave fronthauling technologies also adopted in 5G-XHaul.

This work took inputs from the overall 5G-XHaul architecture specified in deliverables D2.1 and D2.2, and included additional definition of specific requirements such as extensive data rate, system scalability, potential reach, resilience, latency and other features needed. These requirements drove the design of the system level architecture as well as the development of the associated systems.

1. Introduction

The upcoming 5G evolution, as well as the higher data rate demand and the multi-service convergence, impose an imminent reformation on the radio access network (RAN) infrastructure. In the 5G era, most radio signal processing in the baseband unit (BBU) will be centralized, in order to ease the implementation of the advanced 5G radio access technologies (RATs), and also to reduce the CAPital EXpenditures (CAPEX) and OPerational Expenditures (OPEX) of the remote radio head (RRH), which only performs the RF-band/baseband conversion. However, such a functional split between the BBU and RRH might provoke a much higher line rate than the actual data rate in the transport link, commonly known as the fronthaul (FH) [1]. In addition, the use cases of 5G are very diverse in terms of the throughput, latency, jitter, device density, etc. this heterogeneity will lead to the coexistence of different RATs. Therefore, the 5G fronthauling will also require more flexible topologies and improved performance [2].

Fronthaul requires protocol transparency since in most cases, it is based on protocols like the common public radio interface (CPRI). In certain radio applications, it also has a stringent latency requirement. This includes emerging wireless techniques like beamforming or cooperative multipoint. Since mobile backhaul (BH) is normally based on Ethernet, the converged front- and backhaul must be compatible with any of the related protocols.

A possible cost-effective solution to satisfy high bandwidth demands as well as protocol transparency are multi-wavelength passive optical network (PON) systems. Here two types of optical distribution networks (ODNs) can be distinguished. First, power-split ODNs are based on wavelength-agnostic power splitters, broadcasting all wavelengths to each optical networking unit (ONU). They are employed in PON systems based on time-division multiple access (TDMA) like G-PON [3] or NG-PON2 [4]. Second, a wavelength-filtered ODN, on the other hand, uses wavelength-division multiplexing (WDM) filters for routing (pairs or groups of) wavelengths to the respective clients.

WDM-PON can support high levels of scalability, transparency and reach. The latter can be increased with optional reach extenders (i.e., optical amplification). To ease the field installation and maintenance, the ONUs in the WDM-PON preferably use wavelength-agnostic transmitters [5], meaning that the wavelength of an ONU does not need to be known a priori. Wavelength-agnosticism can be achieved by either seeded reflective transmitters or tuneable lasers. Given the fact of high bandwidth × reach product and higher tolerance to reflections, the proposed FH solution utilises low-cost tuneable lasers [6], [7].

International Telecommunication Union-telecommunication standardization sector (ITU-T) study group 15, question 6 (Q6), is working on the standardization of such a tuneable-laser-based WDM-PON system in the draft recommendation G.metro. Proposals currently discussed in Q6 include the use of upstream pilot tones (PTs) for wavelength tagging and control, and the use of a downstream communications channel that is transparently attached to all individual wavelengths. In NG-PON2, a similar signalling channel is defined for the point-to-point WDM overlay system, which is called auxiliary management and communications channel (AMCC) [8].

In this document, we first elaborate a flexible FH architecture in detail based on the wavelength-agnostic WDM-PON, in which different resources can be assigned on demand from the BBU to the RRH. In Section 3, we discuss the tuneable transmitter technologies, which will be critical for this FH application, and then explain the system running procedure. In Section 4, we thoroughly analyse the performance of WDM-PON system using an AMCC in the downstream and PTs in the upstream, considering the major related impairments. For the future proofing of beyond 10 Gbps per wavelength, in Section 5, we demonstrate 26 Gbps capability on the same 10G tuneable transmitter by leveraging the advanced modulation format. Section 6 will conclude the document.

2. Overview of Fronthaul in 5G-XHaul Data Plane

To meet the aforementioned requirements, in the ongoing 5G-PPP project 5G-XHaul [9], we propose such a passive WDM technology to flexibly provision the optical FH between the RRH at the antenna tower and the BBU at the central office (CO), as illustrated in Figure 1. The idea is to leverage the PON technology in order to cost-effectively deliver the FH data (e.g. CPRI or Ethernet) for massive radio cells, while the baseband processing is centralized and shared at the CO.

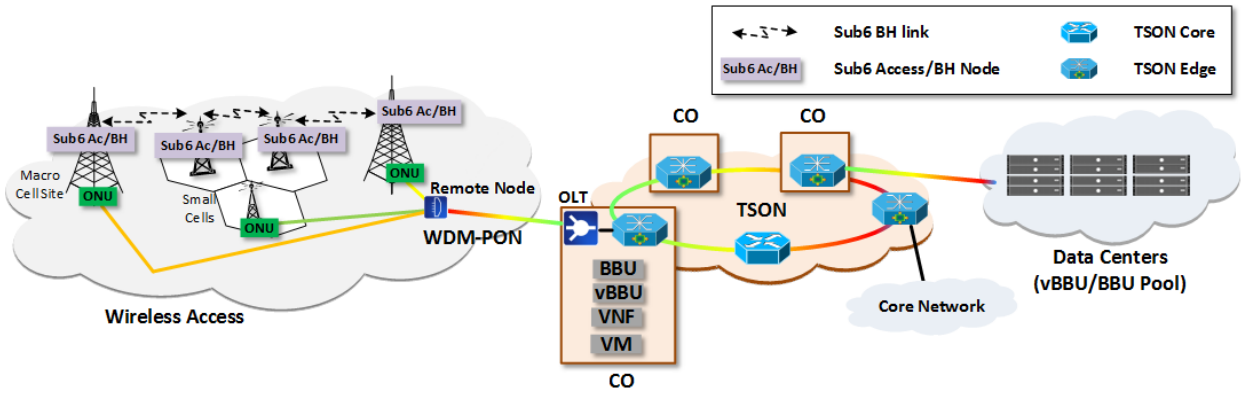

Figure 1: Overview of the WDM-PON-based FH link in the 5G-XHaul project.

The WDM-PON FH is designed to deliver a wavelength-based point-to-point (P2P) connectivity between BBUs and RRHs. Each WDM wavelength is currently able to achieve bit rates at least 10 Gbps bidirectionally, over a transmission distance of 20 km. Since the dark fibre is at a premium especially in the dense urban area, single fibre working (SFW) is becoming increasing critical. Therefore, the downlink operates at the L-band while the uplink operates at the C-band.

2.1 Flexible Fronthaul Architecture

Current Cloud-RAN architectures (e.g. LTE) connect at any given moment one BBU to one RRH, which is suboptimal from an energy-consumption point of view, but in some cases it may be also suboptimal in terms of performance. For instance, some of the new RATs like fractional frequency reuse (FFR) or coordinated multipoint (CoMP) require the transmission of different radio frames from different RRHs [9]. Therefore, we introduce a cross-connect between the BBUs and the client side of the optical line terminal (OLT), as depicted in Figure 2. The WDM-PON system serves for FH transmission by connecting the BBUs at the OLT to the RRHs attached to the ONUs, where the traffic flow of each RRH can be flexibly connected to a different BBU by changing the BBU-OLT transceiver connection in the cross-connect.

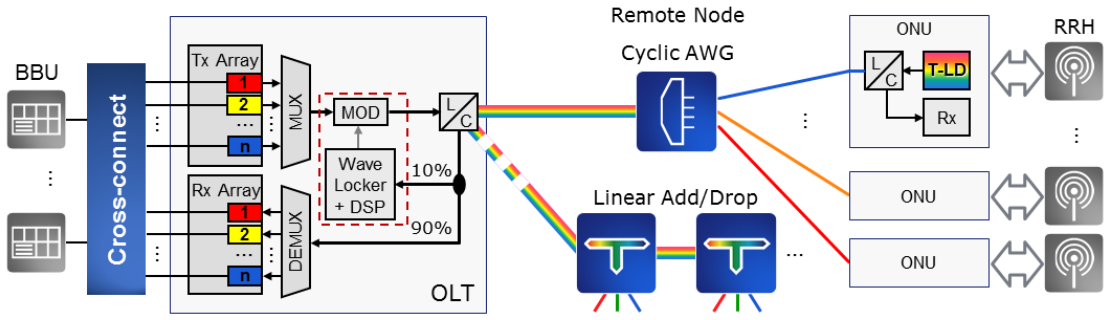

Figure 2: WDM-PON system architecture flexibly connecting RRHs with BBUs.

To realize the cross-connect a transparent solution can be provided, for instance, by an optical fibre switch. This type of switch is available with the size of up to 384 × 384 ports. The advantage of an optical switch is data rate and format transparency, such that the CPRI, Ethernet or Optical Transport Network (OTN) signal of any rates can be switched. Also, the switching power is typically low and does not depend on the rate of the signal. Alternatively, electrical switches can be utilized in the cross-connect. However, these switches are often

rate or format specific, or they might terminate the protocol of the Layer-2 signal. On the other hand, they provide a lower cost solution and can be implemented with a smaller footprint.

Ideally, the arrayed waveguide grating (AWG), as the RN that splits and routes the wavelengths, should be located in the field close to all the RRHs, namely in a tree structure. In some cases, however, installing the RN in an optimal location is quite difficult in practice. Alternatively, the add/drop line structure can be adopted, where the individual wavelength or group of wavelengths is added and dropped at the distributed filter nodes along the trunk line. Both structures are depicted in Figure 2. The add/drop line structure could also add fibre protection by terminating both ends of the line at the CO.

2.2 System Concept with Remote Wavelength Control

As also shown in Figure 2, to autonomously configure the wavelengths of remote ONUs, a centralized wavelength locker is implemented in the OLT, which is able to communicate with each ONU via an out-of-band communication channel and set the ONU wavelength automatically according to the connected port at the RN [10], [11]. More importantly, such an implementation will also significantly reduce the cost of tuneable ONU lasers, because each of them no longer needs a dedicated wavelength locker, instead, they can share this centralized locker [6].

Another crucial cost component of the tuneable laser, however, is the calibration of the injection current for each operating wavelength – and for uncooled devices over the full operating temperature range [12]. Especially for a higher number of tuning currents, this can be time consuming and correspondingly quite expensive in production. The precise wavelength calibration can be avoided by using the centralized wavelength control, in a way that ONU lasers do not need to be sufficiently calibrated, but need to continuously sweep over the operating wavelength range upon turn-on.

At the OLT, fixed or tuneable lasers might be used. Tuneable lasers would reduce spare stock, while fixed lasers possibly are cheaper. A future option would be the use of transceiver arrays with fixed wavelengths.

A low-bit-rate signalling channel can be implemented in the overhead of several communication protocols. However, this approach requires protocol termination in the ONU, which would severely limit the applications of the WDM-PON system due to protocol opaqueness. Therefore, the preferred solution is an AMCC modulated transparently onto each optical channel. Similarly, upstream channel tagging can be done with the PT. The detailed implementation of both the AMCC and PT will be elaborated in Section 4.

For start-up of a new ONU, the OLT sends the PT frequency and target wavelength via the AMCC to the ONU. During start-up, the ONU transmitter modulates its PT with the assigned frequency onto the continuous wave (CW) light. The ONU then starts tuning its wavelength without data modulation. As soon as the OLT detects the ONU pilot-tone frequency in one of the receivers, it informs the ONU via the AMCC. Having reached the correct channel, upstream data transmission begins, while the ONU modulates the PT onto the payload data and the wavelength fine-tuning is subsequently performed by the centralized wavelength locker, and the control information is still sent via the AMCC. Some wavelength tuning algorithms are proposed in [13][14][15].

Figure 3 illustrates this initial wavelength tuning of the ONU laser, where the blue line indicates the track of the wavelength tuning and the orange curve represents the corresponding changes on the received optical power at the OLT.

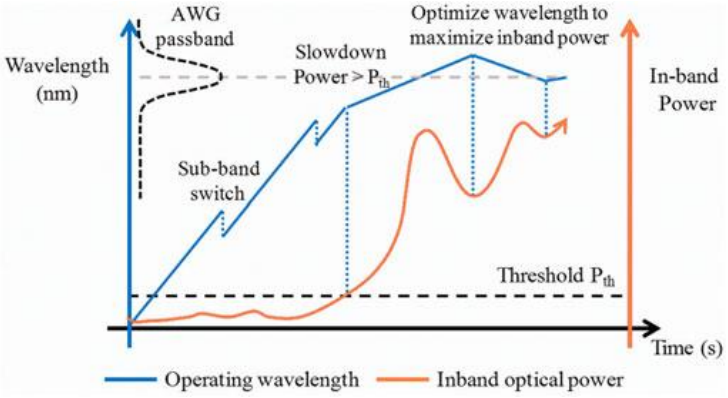

Figure 3: Initial wavelength tuning based on the feedback of received power.

AMCC and PTs lead to certain penalties on the payload, and vice versa. Amplifiers in the OLT can influence the PTs as well. Finally, lasers without full calibration can lead to crosstalk in already established upstream channels during start-up. All these effects are analysed in Section 4.

For ONU monitoring and management, an AMCC can also be used in the upstream. This is done, e.g., in NG-PON2 and is also intended to be included in G.metro. A similar tuning process can be used for tuneable OLT lasers with little extra efforts.

3. Optical Transceivers for Fronthaul

A key component for the low-cost network is a tuneable laser, required in the remote colourless interfaces. While several solutions have been implemented and introduced in T-SFP+ modules, some of these components need to be re-designed to enable a low-cost solution. These lasers must be reduced considerably in cost and complexity as compared to today's tuneable XFP/SFP+ modules, while still capable of 10 Gbps data rate over up to 20 km transmission distance.

3.1 Tuneable Laser Requirements

To make tuneable lasers more attractive and even feasible for the low-cost WDM-PON system, still several critical requirements have to be carefully considered, which are clarified in the following subsections.

3.1.1 Low Cost

Tuneable laser diodes for the mass-deployed FH must become competitive, compared to the current deployment where grey-light or CWDM transceivers are dominant. The potential for the low-cost mass production correlates with the number of sub-components or laser chip sections which are required for the transmitter, and the potential for monolithic integration, sufficient on-wafer testing and the avoidance of complex per-laser calibration processes.

An important contribution to the overall tuneable laser cost comes from the embedded wavelength locker/etalon filter (costs not only stem from the material costs but also and to an even larger contribution from assembly costs). That is why it makes sense to replace the individual wavelength locker in each laser by a centralized implementation with only one locker in the OLT being shared by all attached ONU devices.

Furthermore, reducing the effort for laser calibration can also relax laser production, where only coarse tuning curve may be required, and the precision of actual wavelength can be mitigated by the system-level wavelength locking.

Another factor to save costs and reduce the power consumption of lasers is to operate them without a thermoelectric cooler (TEC). Uncooled operation of distributed Bragg reflection (DBR) lasers has been shown with operation temperatures up to 90 °C [16]. Instead of a TEC, a simple heater may be used to fix the temperature of the laser chip within a certain (relatively high) temperature range. Removal of the TEC also allows lowering the power dissipation (of the SFP module) to below 1 W.

3.1.2 Stability over Time

In the absence of a dedicated wavelength locker, even the laser currents can be measured, the emitted wavelength may still be drifted from the central grid. Though this drifting will be compensated by the centralized wavelength locker, a relatively stable free-running wavelength only requires periodic remote control loop with longer time interval, which relaxes the signal processing effort in the centralized wavelength locker. Without the wavelength locker but under a constant temperature, typically, the DBR laser deviates about 1 GHz per 20 hours after warm-up.

3.1.3 Simple Tuning Mechanism

Tuning-control complexity is also of major concern. This relates to the number of laser-chip sections which need to be controlled simultaneously (potentially creating multi-dimensional tuning maps with mode hops), and number of electrodes which are required. Simpler and more reproducible the wavelength tuning map is and the smaller number of control currents or voltages the laser has, the simpler system integration and components packaging will be.

3.1.4 Tuning Range

In order to achieve lowest cost tuneable lasers, C-band wavelengths would be preferable. It was also recognized that the boundaries of the C-band are not rigidly fixed and a limited amount of potentially more costly lasers at the extended edges of the C-band could potentially still provide an overall attractive configuration.

For the first application proposed in G.metro, in total 20 bidirectional DWDM channels with 100 GHz frequency spacing (defined in ITU-T G.694.1) operate only in C-band, where the downstream uses the grids from 196 THz to 194.1 THz (i.e. 1529.55 nm to 1544.53 nm), and the upstream occupies the range from 192.9 THz to 191 THz (i.e. 1554.13 nm to 1569.59 nm). Lower wavelengths are used in downstream for allowing the use of commercial erbium-doped fibre amplifiers (EDFAs) at the OLT, and the guard band in between (9-10 nm) would allow workable solutions to separating downstream and upstream directions. The requirement of such

a half-C-band tuneability will help the manufacturers simplify the fabrication and consequently reduce the overall cost. For instance, the simple three-section DBR lasers have a limited tuning range of up to 14 nm.

However, when scaling up to the 40-channel application, the tuneable ONU lasers have to cover the full C-band for the upstream (ideally at the same cost), while the downstream is shifted to L-band accordingly.

3.2 Available Laser Technologies

Generally, there are different options to implement such a device, which can be divided into electronic, thermal and mechanical tuning. The most common implementations of electronically tuned lasers are different implementations of DBR lasers. For mechanical tuneability, progress is achieved especially in micro-electromechanical vertical cavity surface emitting lasers [17], [18]. For thermal tuning, narrow-band (approx. 5 nm) tuneable distributed feedback (DFB) lasers are in general available.

3.2.1 Distributed Bragg Reflection (DBR) Lasers

The tuneability of DBR lasers is achieved by electronic tuning, which refers to the application of an electric field or an electric current that modifies the refractive index and, in turn, modifies the laser frequency. Several derivatives of DBR lasers are available, such as the Y-branch laser, three-section DBR, sampled grating DBR laser (SG-DBR), digital supermode DBR laser (DS-DBR), grating-assisted co-directional coupler laser with sampled grating reflector (GCSR), etc. The DS-DBR and SG-DBR lasers are capable of tuning over the full C-band, while the three-section DBR laser may only cover a half C-band. Two examples (DS-DBR and Y-branch lasers) are shown in Figure 4.

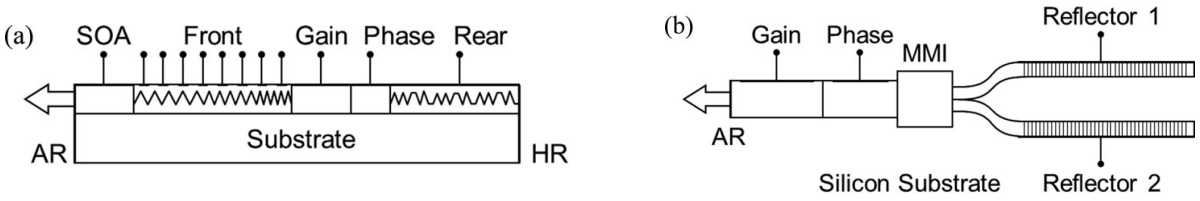

Figure 4: Wideband-tuneable semiconductor laser types (a) 5-section DS-DBR laser; (b) Sampled-Grating Y-branch laser.

Early full C-band tuneable lasers based on a modulated grating Y-branch laser were reported [19]. Four control currents are required to provide gain pumping, perform the tuning of two gratings and to align the phase. A successor of this laser type is commercially available.

Another, also full C-band tuneable laser, based on multiple band reflection filters [20] also requires four injection currents for gain pumping, phase control, and tuning of two gratings. One of the currents is switched between different gratings, reflecting different parts of the spectrum [12]. A variant of this laser is also commercially available. Both of these lasers can be coupled to an external modulator either monolithically or in a hybrid-integrated way. A dispersion-limited transmission range of 80 km can be achieved without chromatic dispersion compensation.

3.2.2 Micro-Electromechanical System Vertical Cavity Surface Emitting Laser (MEMS-VCSEL)

Next to electronically-tuned multi-section DBR lasers, MEMS-VCSELs are on the way of becoming a relevant wideband-tuneable laser source. MEMS-VCSELs consist of a VCSEL (with its potentially broad gain region), complemented by a movable mirror to modify the cavity length. MEMS-VCSELs can be integrated monolithically or in a two-chip assembly. They usually have lower output power compared to DBR lasers. For wideband tuning, only a single contact (to the mirror holder) is required, thus making tuning mechanism simpler. In addition, MEM-VCSELs are not subject to (super-) mode jumps.

More recently, tuneable VCSELs have been demonstrated for a tuneability of over 100 nm [21], [22]. In another implementation that we adopted, the tuneable laser diode is based on a long wavelength Indium Phosphide (InP) Buried Tunnel Junction (BTJ) VCSEL and features a MEMS top mirror [23], [24]. A cross section of this VCSEL design is illustrated in Figure 5(a), and the laser has been packaged as a transmitter optical subassembly (TOSA) with a standard LC connector, as shown in Figure 5(b). The short cavity length of these lasers enables a large mode-hop free tuning range. For these lasers, only two tuning currents are required, for gain pumping and to control the cavity length via a micro-movement of one facet. However, due to the typical chirp of VCSELs, the dispersion tolerance of the transmission is limited to about 10 km for a 10 Gbps signal. It has

been shown, however, that by over-compensating the chromatic dispersion a transmission range of 0 to 40 km over standard single mode fibre (SSMF) can be achieved [25].

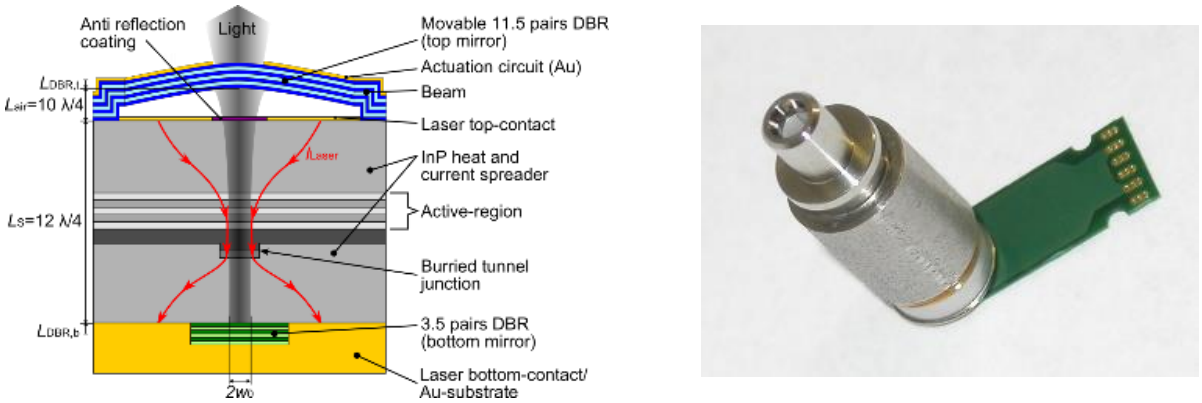

Figure 5: (a) Cross section description of MEMS-VCSEL; (b) Photo of packaged LC-TOSA.

Another similar tuneable MEMS-VCSEL assembled in a standard SFP+ form has already been demonstrated on a converged front- and backhaul testbed within the project [26]. The MEMS-VCSEL SFP+ operates in the C-band with a capacity of 10 Gbps, and a MEMS-actuated mirror on top of the VCSEL enables a tuneability of 13 nm [27].

The tuneable VCSEL is a much lower cost and power consumption option than used in other commercially available tuneable transmitters, thanks to its simpler tuning and testing (single control voltage), as well as simpler epitaxy and fabrication processes.

With designs that allow the avoidance of TECs and per-transmitter wavelength lockers, multi-section DBR lasers and MEM-VCSELs could have similar mass production potential.

3.3 Future Developments

To enable a full integration of the ONU optical engine, ultimately the tuneable, photo-detector and even up-/downstream splitter can be integrated on a same platform. Recently, a tuneable laser based on a polymer platform has been demonstrated, where the temperature tuneable grating was realized in the polymer and an InP based gain chip was hybrid integrated [28]. This photonic integrated circuit (PIC) also contained the band splitter required to separate the signal directions and a receiver photodiode. While three tuning currents are required for gain pumping, phase control and heating of the tuneable grating, the tuning range of a single grating covered half of the C-band, sufficient for the initial application proposed in the G.metro draft.

4. Enabling Technology: Passive Wavelength-Agnostic WDM

In Section 2.2 we introduced the working concept of an OLT-based wavelength control, where the ONU laser keeps sweeping until it reaches the wavelength of the filter port (AWG or add/drop) connected. The OLT will then detect the ONU signal and confirm this to the ONU via the management channel. In this section, we will thoroughly analyse the performances of downstream AMCC and upstream PT, respectively.

4.1 Downstream Analysis

The AMCC modulation can be implemented by the amplitude-shift keying, phase-shift keying, or frequency-shift keying modulation. Direct envelope modulation of digital data onto the optical channel is an efficient alternative in terms of effort and cost. It needs a certain modulation depth to achieve sufficient bit-error rate (BER). On the other hand, it reduces the eye opening and leads to a power penalty of the payload.

In the following subsections, we evaluate the implementation details of the AMCC, and the impairments caused by data payload onto the AMCC and vice versa.

4.1.1 AMCC Requirements

An AMCC transports control commands for tuning the ONU laser. To avoid wrong tuning of the ONU transmitter, errors in the AMCC must be corrected or at least detected in order to discard the message. In the G.metro, an AMCC with 64-bitmessages and extended Hamming code has been discussed. Seven parity bits are added to 57 payload bits, resulting in a Hamming distance of 4. As a result, single errors can be corrected, and double and some triple errors can be detected and the message can be discarded.

Assuming 64-bit messages and an AMCC bit rate of 100 kbps, the mean time between discarded and erroneous messages are calculated as shown in Table 1.

Dropped messages only cause delay in the tuning process because the ONU waits for the next message. Erred messages, in contrast, can lead to mistuning and should be avoided. A BER of 2×10^{-6} at 100 kbps leads to some triple errors or more every ~125 years, which cannot be detected leading to erred and un-discarded messages.

4.1.2 AMCC Performance

The measurement setup to evaluate the AMCC performance is shown in Figure 6. An optical signal at 2.5 Gbps carrying a pseudo-random bit sequence (PRBS) of length 2^{31}-1 (PRBS-31) is amplitude-modulated with the AMCC data using a Mach-Zehnder modulator (MZM). The combined signal is split and one portion is used to measure the eye diagram to evaluate the AMCC modulation depth. The second portion is split again to measure the BER of the payload and of the AMCC as a function of the received power. The AMCC modulation depth is defined as the peak-to-peak power variation of the payload "one" rail divided by the maximum payload "one" rail power.

Table 1: Mean times between dropped and erred messages.

Message channel BER	Mean time between dropped messages[1]	Mean time between erred messages[2]
10^{-6}	3.6 days	893 years
$2\cdot10^{-6}$	22 h	125 years
$5\cdot10^{-6}$	3.5 h	7.8 years
10^{-5}	53 min	1 year
$2\cdot10^{-5}$	13 min	44 days
$5\cdot10^{-5}$	2 min	3 days
10^{-4}	32 sec	8.6 h

[1] Based on the probability of two-bit errors in a message plus half the probability of three-bit errors in a message.
[2] Based on half the probability of three-bit errors in a message plus probability of four or more bit errors in a message.

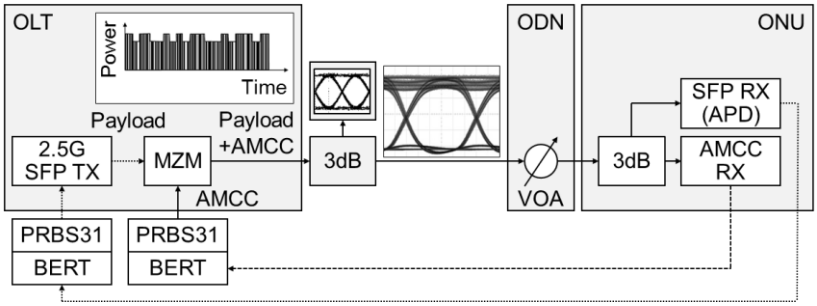

Figure 6: Measurement setup for AMCC sensitivity evaluation under the influence of the payload and vice versa. The eye-diagram inset shows a 2.5 Gbps payload signal with a 100 kbps NRZ envelope modulation.

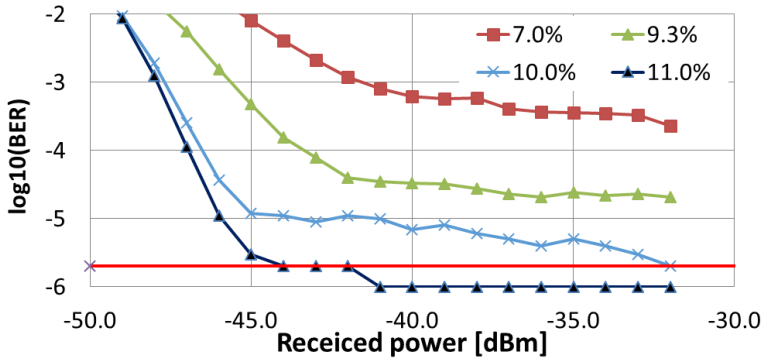

Figure 7: BER vs. received power of an envelope modulated 100 kbps message channel. The modulation depth is varied from 7% to 11%.

The AMCC sensitivity was measured as a function of the received power for 100 kbps non-return-to-zero (NRZ) modulation and for various modulation depths under the impact of a 2.5 Gbps PRBS-31 payload. The data rate 2.5 Gbps with PRBS-31 was chosen as the payload with lowest expected frequency content. While GbE as well as low CPRI rates are 8B/10B coded, the uncoded 2.5 Gbps modulation is the most stressing payload data.We verified that the performance of the AMCC is far better for 10.7 Gbps, PRBS-31 or 1.25 Gbps, PRBS-7 payloads.

Figure 7 shows the BER of the AMCC for modulation depths between 7% and 11%. For all modulation depths, an error floor is observed. We associate this error floor with the spectral components of the payload falling into the AMCC receiver bandwidth. In other words, the on-off modulation of the payload acts like noise on the AMCC and is increased with increasing power level. Only for higher AMCC modulation depths, the relative noise is reduced.

As described above, a BER of at least 2×10^{-6} is required to ensure an acceptable performance of the AMCC (red line in Figure 7). A modulation depth between 10% and 11% is required for this BER, and a received power of around -40 dBm is necessary.

The NRZ format is not fully optimum for the AMCC due to a necessary clock for data recovery. A modulation format including the clock is preferred in terms of cost-efficiency and simplicity. Manchester coding supports clock recovery from the transmitted data. One drawback is the bandwidth demand, which is twice as high as for NRZ. The AMCC error floor for Manchester coding is shown in Figure 8 as a function of the modulation depth at a received power of -35 dBm.

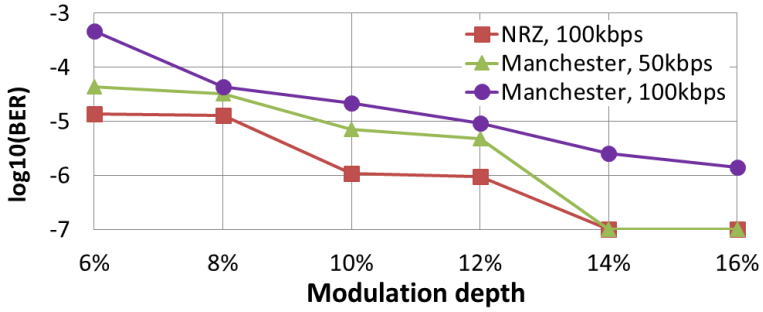

Figure 8: Error floor as function of the modulation depth at -35 dBm for 100 kbps NRZ encoding compared to 50 kbps and 100 kbps Manchester encoding.

We transmitted 2×10^7 bits for each data point. BER values of 10^{-7} indicate bit-error-free transmission. 100 kbps NRZ and 50 kbps Manchester-coded signals show similar performance. Both encoding schemes show a BER floor better than 10^{-6} for a modulation depth of 14% and above. The 100 kbps Manchester-encoded AMCC suffers more from the interaction with the payload, as explained above. An error floor of 10^{-6} is not achieved for modulation depths below 16% and, therefore, Manchester-encoded 100 kbps AMCC was not evaluated further.

Next, we evaluate the sensitivity of the payload in presence of an AMCC with Manchester and NRZ encoding.

4.1.3 AMCC Impact on Payload

Envelope modulation of the AMCC reduces the eye opening of the payload as a function of the modulation depth of the AMCC. An appropriate AMCC performance requires a modulation depth between 10% and 14%, depending on the modulation format and AMCC bit rate.

For evaluation of AMCC impact on payload, the same setup was used as for the AMCC sensitivity measurements, see Figure 6. The receiver sensitivity was measured for a 2.5 Gbps signal in the presence of an AMCC with 10% and 15% modulation depth. A modulation depth of 15% was chosen to have some additional safety margin for the AMCC. The BER versus received payload power in presence of an AMCC with 100 kbps NRZ and 50 kbps with Manchester coding is shown in Figure 9(a) for 10% modulation depth and in Figure 9(b) for 15%, respectively.

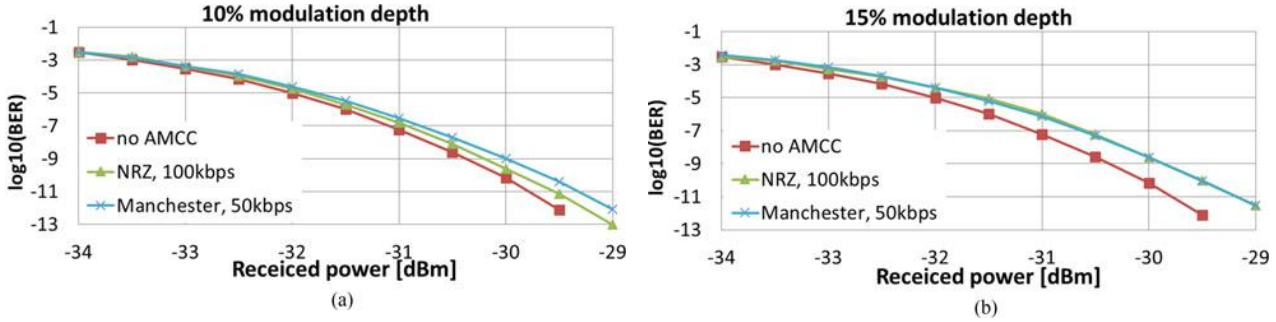

Figure 9: Bit error rate of the 2.5 Gbps payload channel vs. received power with (a) 10% and (b) 15% modulation depths of the envelope modulation. "No AMCC" is the case without envelope modulation.

The AMCC impact on the payload only marginally depends on modulation format and data rate. At a payload BER of 10^{-12}, the power penalty due to an AMCC with 10% and 15% modulation depth is below ~0.5 dB and ~1 dB, respectively.

4.2 Upstream Analysis

In this section, we compare two implementations of the PT envelope modulation and their impact on the payload. We also analyse the impairments on the PT due to the adoption of an EDFA.

4.2.1 Pilot Tone Generation

In the upstream direction, a PT is modulated on each channel for wavelength control at the centralized wavelength locker. Considering low-cost implementation, we evaluated two intensity modulation methods shown in Figure 10.

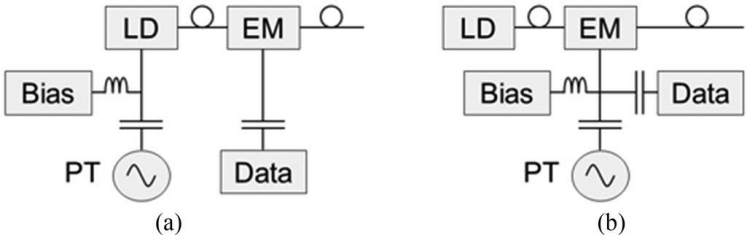

Figure 10: Pilot tone generation: (a) Adding a small sinusoidal current to the laser's bias current; (b) dithering the bias voltage of external modulator.

Multiplicative PT modulation: Figure 10 (a) shows the block diagram for modulating the PT directly on the laser bias current while the payload data $d(t)$ are modulated via an external modulator. The resulting power $P(t)$ can be formulated as

$$P(t) = \hat{P} \cdot [1 + m \cdot \cos(2\pi f_{tone} t)] \cdot d(t) \quad (1)$$

$\hat{P}$ is the unmodulated laser output power, f_{tone} the PT frequency, and m the modulation index of the PT. The PT modulation depth m is defined as

$$m = \frac{P_{\max} - P_{\min}}{P_{\max} + P_{\min}} \quad (2)$$

P_{max} and P_{min} are the maximum and minimum optical power during a mark rail due to superimposition of the PT.

In this modulation scheme, the PT is introduced as a multiplier to the data, resulting in a convolution of the PT spectrum with the data spectrum. The same result would be obtained by modulating the PT onto the payload signal via an external modulator or a variable optical attenuator (VOA).

Additive PT modulation: Figure 10 (b) shows PT-induced dithering of the bias voltage of an external modulator. Adding the PT to the bias of an external modulator can be expressed as

$$P(t) = \hat{P} \cdot [d(t) + m \cdot \cos(2\pi f_{tone} t)] \quad (3)$$

The power spectral density of the PT is linearly added to the data spectrum. This results in an additional line in the data spectrum.

4.2.2 Pilot Tone Impact on Data – Simulation

PT modulation causes a power penalty of the data signal. The additive PT modulation has the benefit that the PT can be filtered out when the PT frequency is below the lower cut-off frequency of the payload receiver, which is formed by the AC coupling and the trans-impedance amplifier (TIA) input impedance. Then, the data signal remains undistorted. For multiplicative PT modulation, mixing products of PT and data are present in the whole data spectrum.

Four different situations are shown in Figure 11. The left column shows the cases for PT frequencies below the lower cut-off frequency of the receiver band-pass characteristic $f_{g,HP}$. The slowly varying PT is dropped at the receiver input filter (AC coupling and TIA input impedance), which corresponds to a decision threshold DT(t) for the data signal which follows the PT. For PT frequencies exceeding the lower cut-off frequency (right column), the decision threshold does not follow the average signal and remains constant, leading to non-optimum threshold.

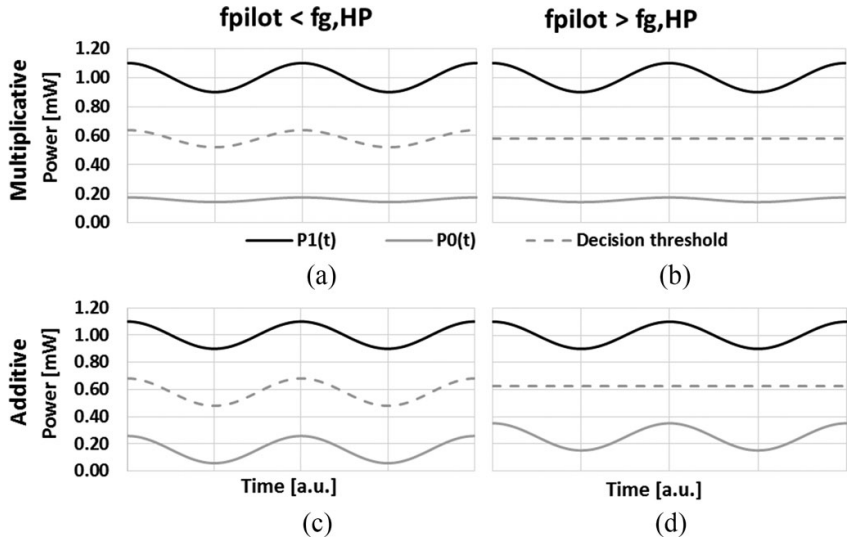

Figure 11: Time-resolved PT modulation of mark P1(t) (black) and space P0(t) (grey).Upper row: multiplicative modulation; bottom row: additive modulation. Left column: PT frequency below lower cut-off frequency $f_{g,HP}$ (decision threshold (dashed) follows average power); right column: PT frequency above lower cut-off frequency $f_{g,HP}$ (decision threshold is constant).

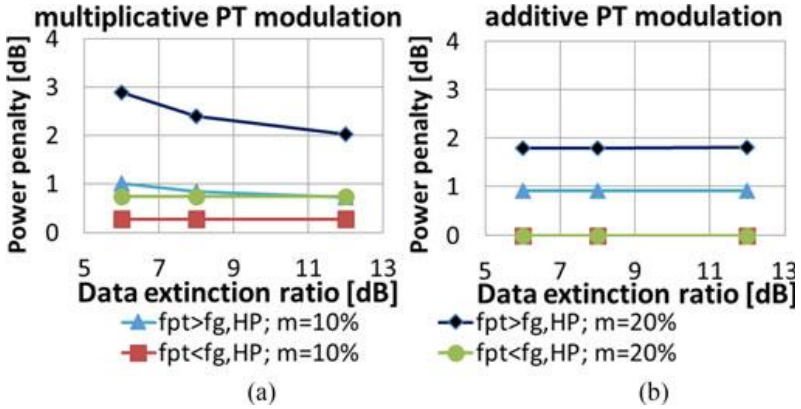

Figure 12: Power penalty of data signal at BER of 10^{-9} as function of the extinction. (a) Multiplicative PT modulation; (b) additive PT modulation (circle and square curve overlay) (*m*: PT modulation depth; $f_{g,HP}$: Rx lower cut-off frequency).

Assuming a Gaussian noise distribution with the same variance σ for mark and space, the BER can be calculated by

$$BER(t) = \frac{1}{2} \cdot \left[\operatorname{erfc}\left(\left| \frac{P1(t) - DT(t)}{\sigma} \right| \right) + \operatorname{erfc}\left(\left| \frac{DT(t) - P0(t)}{\sigma} \right| \right) \right] \quad (4)$$

By averaging the time-resolved BER over one PT period, the power penalty can be derived, as shown in Figure 12. For low PT frequencies and additive modulation, the data power penalties are negligible, whereas for multiplicative modulation, a penalty can be observed. For high extinction ratios and high PT frequencies, both modulation schemes result in comparable power penalties.

4.2.3 Pilot Tone Impact on Data – Measurements

To verify our theoretical results, we used the multiplicative modulation scheme and measured the power penalty for both 2.5 Gbps and 10 Gbps payloads using two different SFPs.

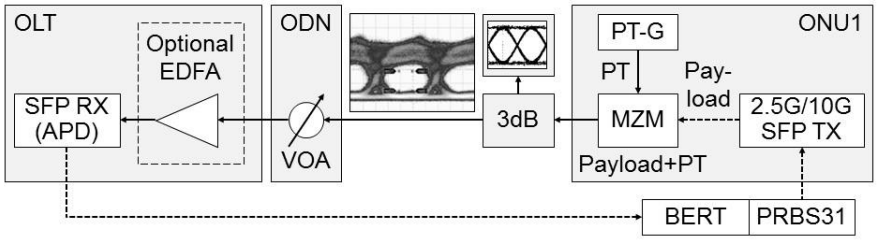

Figure 13: Measurement setup for power penalty evaluation of a PT on a data signal in the case of multiplicative PT modulation scheme.

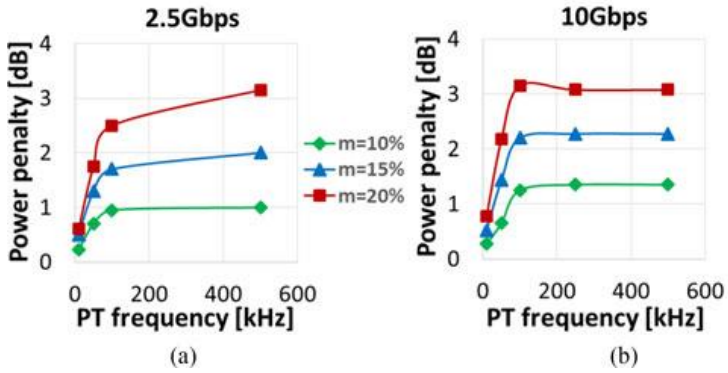

Figure 14: Measured power penalty of data signal as function of the PT frequency for different modulation depths. Left: 2.5 Gbps; right: 10 Gbps. (*m*: PT modulation depth).

Figure 13 shows the measurement setup. Signals at data rates of 2.5 Gbps and 10 Gbps were modulated with a PRBS-31. The extinction ratio of the data signal was ~8 dB for both SFPs. The PT was modulated via an MZM onto the optical payload signal (i.e. multiplicative scheme). The optical signal was split into two portions. One portion was sent to an analyser to monitor the modulation depth of the PT, the second portion was sent to the receiver of the SFP to measure the BER as a function of the received power.

The power penalties for 2.5 Gbps and 10 Gbps are similar, as shown in Figure 14. Far above the lower cut-off frequency, they remain almost constant. For low PT frequencies, a power penalty is still observed. These results are in line with the theoretically analysed power penalties.

PT frequencies below the lower cut-off frequency and modulation depth of 10% lead to a power penalty of ~0.2 dB. Increasing the PT frequency above the lower cut-off frequency yields a power penalty of ~1.3 dB.

We can conclude that a PT frequency below the lower cut-off frequency keeps the payload power penalty small. Therefore, the lower cut-off frequency of the SFP can be used as an upper bound for the PT frequency. Regarding payload penalty, the PT modulation depth should be 10% or lower. In the experiments, the detection of a PT with 10% modulation depth successfully tested. However, the PT detection depends heavily on receiver electronics and were not further evaluated.

4.2.4 Pilot Tone in Amplified System

Optical amplification for reach extension is a possible option. EDFAs at the OLT still keep the RN passive and can extend the reach. However, an EDFA can affect the PT in several aspects. Saturated EDFA carrier dynamics can reduce or cancel the PT modulation. Furthermore, cross gain modulation (XGM) can imprint a PT on all other channels, which would lead to PT detection in wrong channels. The EDFA gain control can partly negate these effects.

In the experimental evaluation, the PT was modulated on a tuneable laser emitting at 193.9 THz. The PT modulation depth into the EDFA was set to 20% and was measured again after the EDFA. An unmodulated control channel emitting at 194.3 THz was launched into the EDFA as well. The impact of an EDFA on the modulation depth of the PT is shown in Figure 15(a). For evaluation of the influence on the modulation depth of the PT, the power difference ΔP between the PT channel and the unmodulated control channel was varied between 8 dB and 26 dB. This power difference has negligible effect, and the plots almost coincide. Two extrema are visible. At 5 kHz, the PT modulation depth is increased to 20.5% and at 10 kHz, it is reduced to

19.25%. Increasing the PT frequency further, the modulation depth approaches its former modulation depth value of 20%. Considering a PT modulation depth margin of ±1% points leads to no PT-frequency restrictions.

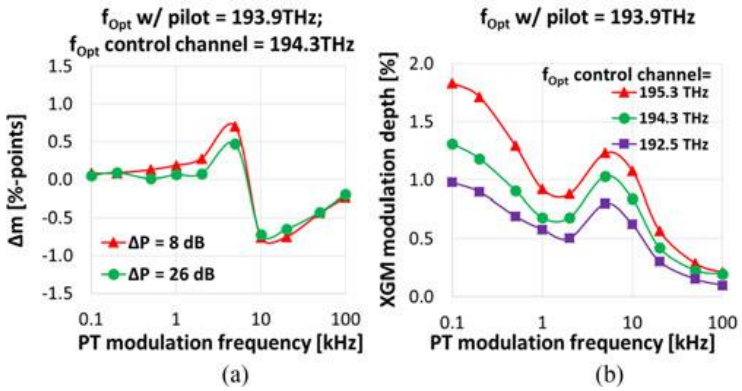

Figure 15: EDFA impact on pilot tone (a) modulation-depth change Δm; (b) XGM.

Amplifier XGM can imprint a PT on all other channels and cause ghost tones. XGM versus PT frequency is shown in Figure 15(b) for different wavelengths of the unmodulated control channel. The power difference was varied as well. However, for clarity, we selected only the power difference with the highest XGM. We observe that the control channels emitting at short wavelengths are most affected by XGM. This is also confirmed by other wavelength configurations. This seems reasonable due to the EDFA gain profile, which shows higher gain for shorter wavelengths. To keep the XGM below 1% would require a lower limit of the PT frequency of 20 kHz.

4.3 Channel Crosstalk during Tuning

So far, we only considered fixed-wavelength or fully calibrated tuneable lasers, which can immediately emit on the correct wavelength. Due to the low-cost requirement, the tuneable lasers might not be fully calibrated since this is a time-consuming and costly per-sample process. Centralized wavelength locking and related signalling can provide the necessary laser monitoring and control; however, crosstalk can now occur during the tuning process. This happens when a non-sufficiently calibrated laser has to sweep across (parts of) the upstream wavelength band in order to find its correct channel.

In the WDM-PON system, signals outside the target wavelength channel are suppressed by the WDM filters. However, channel isolation can be reduced toward the edges of filter channels and lead to a considerable crosstalk. For example, in the case of two cascaded flat-top AWGs, the provided channel isolation can be as low as 12 dB at half of the channel spacing for neighbouring multiplexer ports. This leads to incoherent cross-talk, as shown in Figure 16.

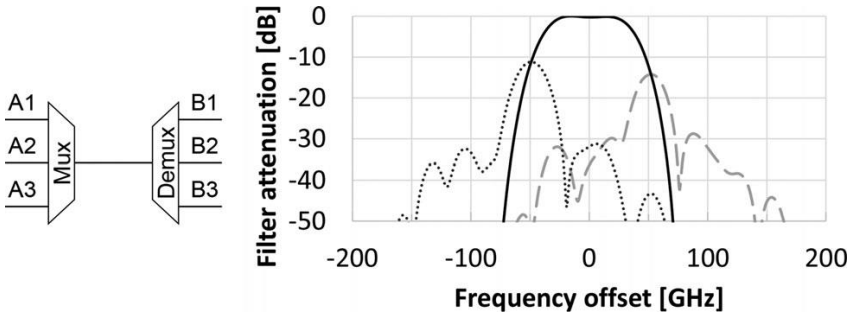

Figure 16: Filter function of two cascaded 100 GHz spacing AWGs. Solid line: Target channel (A2→B2); dotted and dashed lines: crosstalk, when laser is connected to upper and lower neighbouring port of multiplexer filter (A1→B2 or A3→B2).

Channels can differ in launch power and in optical path and insertion losses between the ONUs and the OLT. Reduced channel isolation can have two effects. First, the tuning ONU could be detected misleadingly in the neighbour channel. This can be avoided by assigning different PT labels to each ONU, which are detected by the dedicated OLT receiver. Only if the respective label is detected with an appropriate power level, the ONU surely emits on the correct wavelength channel. Second, during tuning, a strong tuning channel can interfere

with weak working channels, leading to incoherent and coherent crosstalk. These crosstalk effects and mitigation examples are discussed in the following subsections.

4.3.1 Worst-Case Crosstalk Scenario

During the tuning process, coherent and incoherent crosstalk can occur. For coherent crosstalk, the interferer and the working channel have the same nominal wavelength. Coherent crosstalk is suppressed by the multiplexing filter by up to 30 dB. Once passing through that filter, the interferer will not be suppressed any further by the demultiplexing filter. At the OLT receiver, the electrical fields of signal and interferer beat. Therefore, highest coherent crosstalk results for co-polarized signals.

In contrast, incoherent crosstalk mainly occurs at half of the channel spacing. Here, multiplexing and demultiplexing filters suppress interferers with reduced channel isolation. Photodiodes can detect both, the respective channel and the insufficiently suppressed interferers. As shown in Figure 16, the interferers might be suppressed by only 12 dB after both filters.

For crosstalk analysis, the launch-power window ΔP of the ONU transmitter is assumed with 4 dB. The maximum differential path loss (DPL) depends on the maximum system reach. We assume a fibre loss of 0.275 dB/km, resulting in 22 dB DPL for an 80 km system.

With the values stated above, and assuming worst cases, signal-to-interferer ratio (SIR) of 4 dB and -14 dB results for coherent and incoherent crosstalk, respectively.

4.3.2 Experimental Crosstalk Analysis

For crosstalk evaluation, we used the measurement setup shown in Figure 17. A PRBS-31 signal was generated in SFP at a bit rate of 2.5 Gbps. This signal was then split by a 90/10 splitter. The major portion was sent to the SFP receiver via a 3 dB coupler and a VOA for measuring the BER versus received optical power. The minor portion was sent to a wavelength meter. As for the interferer, we used a tuneable laser. We used two interferer schemes, a DC interferer and an interferer with a low pilot-tone modulation frequency. For the DC interferer, the light of the tuneable laser was split in another 90/10 splitter. The minor portion was sent to the wavelength meter to determine the frequency offset. The major portion was combined with the SFP signal in the 3 dB coupler. A polarization controller (PC) was used to align the polarization of the interferer for the worst case. Attenuators (ATT) 1 and 2 were used to adjust the SIR.

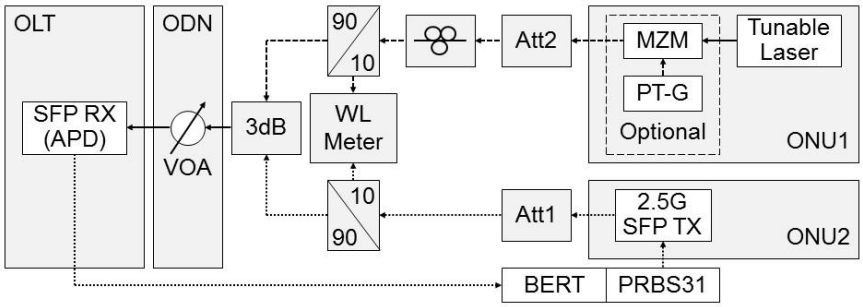

Figure 17: Setup for coherent and incoherent crosstalk evaluation with and without PT modulation.

For modulation with a low PT frequency, an MZM was inserted and modulated by a sinusoidal generator with a modulation depth of 10%.

We studied four crosstalk scenarios:

1. Power penalty over SIR for the incoherent crosstalk (assuming 100 GHz channel spacing and frequency deviation Δf of 50 GHz);
2. Power penalty over SIR for the coherent crosstalk (frequency deviation Δf = 0 GHz);
3. Power penalty over frequency deviation to measure the spectral crosstalk range and transition from the incoherent to coherent crosstalk;
4. Power penalty for a modulated interferer with different PT frequencies for the coherent and incoherent crosstalk.

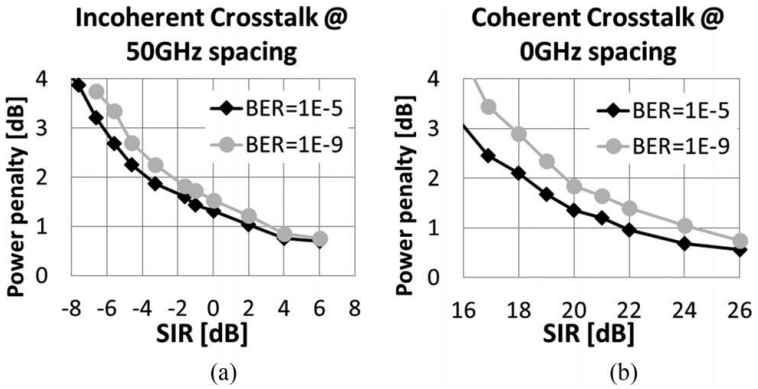

Figure 18: Penalty measurement (a) incoherent crosstalk (Δ*f* ~50 GHz); (b) coherent crosstalk (Δ*f* ~0 GHz) without PT modulation.

We assumed a maximum allowed crosstalk penalty of 1 dB. Figure 18(a) shows the power penalty for the incoherent crosstalk at 50 GHz frequency offset without PT modulation. For a BER of 10^{-9}, the power penalty is below 1 dB for SIR values higher than 3 dB. Therefore, the incoherent crosstalk needs to be improved by up to 17 dB, as the worst-case SIR in the system assumed above is -14 dB.

Figure 18(b) depicts the power penalty for the coherent crosstalk (Δ*f* = 0 GHz). For 1 dB penalty, an SIR of ~24 dB is needed. Since the assumed SIR of the worst-case coherent crosstalk in the system is 4 dB, the SIR needs to be improved by up to 20 dB.

Finally, the interferer was PT-modulated in the multiplicative scheme with 10% modulation depth, and the PT frequency was varied between 1 Hz and 10 MHz. Negligible additional penalty of <0.1 dB was measured for the coherent crosstalk with an SIR of 22 dB over the whole frequency range. For the incoherent crosstalk, we used an SIR of 0 dB. The additional penalty due to the PT is negligible for PT frequencies <10 kHz. For PT frequencies between 10 kHz and 100 kHz, the power penalty rose to 0.25 dB and remained constant for higher PT frequencies. These measurements confirm the results shown in Section 4.2.

In a worst case scenario, the coherent and incoherent crosstalk are ~20 dB higher than the required SIR to keep the power penalty below 1 dB. Several techniques can be applied to mitigate the crosstalk during tuning, e.g., limiting the DPL, power reduction during tuning, reducing the launch-power window, polarization control (scrambling), and /or improving the filter channel isolation. We analysed the aforementioned possibilities and estimate their benefits and drawbacks:

1. Limiting the launch-power window increases the worst-case SIR by ~2 dB. This limited benefit must be related to the cost that results from lower laser yield;
2. Introducing polarization scrambling reduces the required SIR by <3 dB. The additional cost and system complexity of an additional polarization scrambler surpasses its benefit;
3. Improvement of filter channel isolation is limited as well. Isolation depends on filter technology. Increased isolation can have associated negative effects on both, filter cost and insertion loss;
4. The most promising mitigation technique is to reduce the DPL and power during tuning. To maintain certain DPL, the launch power should be reduced during tuning. For directly modulated lasers, launch-power reduction by 20 dB is challenging without hitting the laser threshold current. We assume that 10 dB power reduction is possible for directly modulated laser. Then, limiting the differential reach to 40 km is sufficient to keep the SIR in an acceptable range.

5. Single-Wavelength Capacity of 25G and Beyond

Due to the potential high bandwidth growth in the mobile FH, soon CPRI option 10 (24.33 Gbps) will be necessary to be deployed. The new specification eCPRI has been recently released [29], which enables the use of Ethernet transport. Although eCPRI opens up potential for compression and enhancements needed to meet the increased requirements of 5G, however, still two to three times higher data rates between the BBU and the radio heads will be required.

To facilitate the capacity demand while keeping the lowest cost for the FH, higher order intensity modulation formats with direct detection, such as discrete multitone (DMT) or pulse amplitude modulation with four levels (PAM- 4), allow leveraging the current 10G-class transceiver for much higher data rates.

In this section, we demonstrate a CPRI option 10 capable transmission based on a wideband tuneable MEMS-VCSEL (introduced in Section 3.2.2) over 40 km by using DMT. Results show that DMT modulated on MEMS-VCSEL-based WDM-PON is a viable solution to coping with the future needs.

5.1 DMT Modulation with PT

DMT, as payload data modulation scheme, is based on multiple subcarriers. The subcarrier frequency distance Δf_{Sub} is determined by the (inverse) fast Fourier transformation ((I)FFT) length N and sampling frequency f_S of the digital-to-analogue converter (DAC) by $\Delta f_{sub} = f_S / N$. A 26 Gbps transmission (80 GS/s) and an (I)FFT length of 512 points result in a first subcarrier frequency approximately at 150 MHz. The considered PTs frequency is 3000 times lower than the first DMT subcarrier. Therefore, only a very small penalty is expected due to the huge guard band. However, this applies only if the PT or AMCC is directly modulated onto the laser bias current, leading to an added frequency component in the spectrum. For external modulation, e.g., by a MZM, the PT or AMCC spectrum would be convolved with each DMT subcarrier, leading to higher penalties [30].

5.2 Upstream Measurement Setup

Figure 19 shows the experimental setup. The electrical DMT signal is generated by using offline digital signal processing via Python routines. The used DMT parameters are summarized in Table 2. DMT requires a real valued baseband signal. Hence, an FFT-length of 512 points leads to 255 usable subcarriers at maximum. Therefore, the first subcarrier frequency is at 156.86 MHz leaving enough margin for adding a low frequency pilot tone as proposed in the system concept.

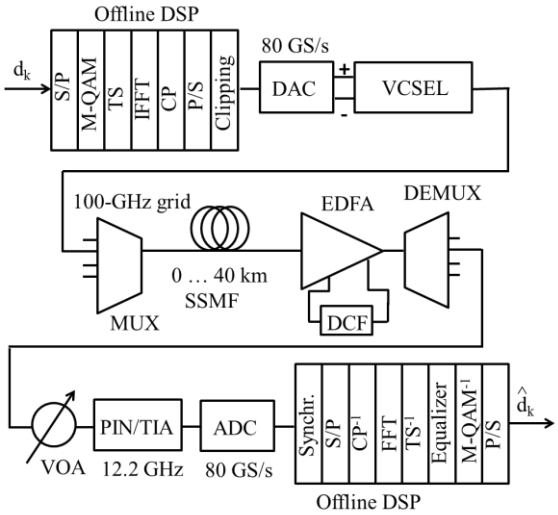

Figure 19: Experimental setup for 26 Gbps DMT transmission up to 40 km SSMF transmission.

Table 2: DMT parameter overview.

Parameter	Value
Cyclic prefix	32 samples
Clipping ratio	9 dB
FFT length	512
TS	5
BL/PL	Levin-Campello
Usable carriers	255

To optimize the transmission performance for each subcarrier, bit and power loading (BL/PL) is implemented using the Levin-Campello algorithm [31]. For this purpose, in a first step, the signal-to-noise ratio (SNR) is estimated by using a 16-QAM constellation with equal power distribution. For high estimated SNR values, a higher-order modulation constellation is loaded onto the respective subcarrier (i.e., up to 16-QAM), BPSK for low estimated SNRs, or even no data are modulated onto the subcarrier if the SNR is below a certain threshold. Additionally, the power of each subcarrier is adjusted to achieve a homogeneous BER for all used subcarriers.

Five training symbols (TS) are added for synchronization and channel estimation. Finally, a 32 sample cyclic prefix (CP) is added and the signal is clipped symmetrically by 9 dB clipping ratio cl_{dB} to reduce the peak-to-average power ratio. The clipped signal $x_{cl}(t)$ is defined by:

$$x_{cl}(t) = \begin{cases} -10^{\frac{cl_{dB}}{20}} \cdot \sigma_x, & \text{if } x(t) < -10^{\frac{cl_{dB}}{20}} \cdot \sigma_x \\ x(t), & \text{if } -10^{\frac{cl_{dB}}{20}} \cdot \sigma_x \le x(t) \le 10^{\frac{cl_{dB}}{20}} \cdot \sigma_x \\ 10^{\frac{cl_{dB}}{20}} \cdot \sigma_x, & \text{if } x(t) > 10^{\frac{cl_{dB}}{20}} \cdot \sigma_x \end{cases} \quad (5)$$

With the unclipped DMT time signal $x(t)$ and the standard deviation σ_x, cl_{dB} was experimentally optimized.

The data rate is fixed to the CPRI option 10 (24.33 Gbps) with 7% forward error correction (FEC) overhead resulting in 26 Gbps gross transmission rate. The shown DMT transmission rates are without TS and CP.

The electrical DMT signal is directly modulated onto the MEMS-VCSEL bias current via a high-speed DAC working at a sampling rate of 80 GS/s. The differential output swing of the DAC is limited to 800 mV. The VCSEL's bandwidth is approximately 7 GHz leading to the bandwidth limitation, and its bias current is optimized for each measured wavelength between 17-19 mA. The high bandwidth DAC was available and used to make sure that no bandwidth limitation is introduced by this device.

The optical wavelength is thermoelectrically tuned between 1530.33 nm and 1561.61 nm. The optically modulated DMT signal is sent to a 40-channel multiplexer with 100 GHz channel spacing, and each channel has an optical bandwidth of 78 GHz leading to no optical bandwidth limitation. The optical signal is then launched into the SSMF at -8 dBm.

After transmission over up to 40 km SSMF the signal is amplified by an EDFA, and the dispersion is compensated with the same dispersion compensating fibre (DCF) for 50 km for all measured reaches. The MEMS-VCSEL is strongly chirped which results in a poor tolerance against the positive chromatic dispersion (CD). The combination of a fix overcompensating DCF in the OLT side and the strong chirp of the VCSEL enables a wide range of the transmission distances. The optical input power for the DCF is kept constant at -4 dBm to avoid nonlinearities in the DCF. Since the DCF and EDFA can be shared between all channels of a WDM-PON system, this approach still supports the low cost requirements for FH applications.

The optical signal is sent through a demultiplexer with similar properties as the multiplexer. One VOA is used to measure the BER over received power input into a linear PIN+TIA receiver with 12.2 GHz bandwidth, leading to further constraints in the electro-optical bandwidth. The opto-electrical converted signal is sent to an analogue-to-digital converter (ADC) with 80 GS/s which is connected to the offline DSP, where the data are recovered and the BER is measured after synchronization and removal of the CP and TS. For all wavelengths and transmission reaches, a low latency interleaved Reed-Salomon Bose-Chaudhuri-Hocquenghem enhanced FEC is assumed. For CPRI's target BER of 10^{-12}, an input BER of $2.26 \cdot 10^{-3}$ is required [32].

5.3 Results and Discussion

For the WDM-PON scheme with centralized wavelength locking, a widely tuneable laser is preferred. We tested different wavelengths, i.e., the first, last, and one channel in the middle of the transmission band. The estimated SNR and bit loading for 0 km and 40 km SSMF transmission are shown in Figure 20.

The usable bandwidth of the VCSEL can be seen from the estimated SNR and bit loading after 0 km transmission shown in Figure 20 (a) and 20(c). The bandwidth was very similar for 1561.42 nm and 1545.32 nm. At 1530.33 nm the estimated SNR is slightly reduced. The bit loading for 1530.33 nm after 0 km transmission is shown in Figure 20(c). The first subcarrier is not used due to AC coupling effects at both transmitter and receiver side. The usable bandwidth is approximately 10 GHz. Figure 20 (b) and 20(d) show the combined transmission effects and bandwidth limitation after 40 km transmission. Although the estimated SNR is reduced, the bit loading schemes for 0 km and 40 km are very similar. A dispersion notch cannot be seen due to the bandwidth limitation of the VCSEL.

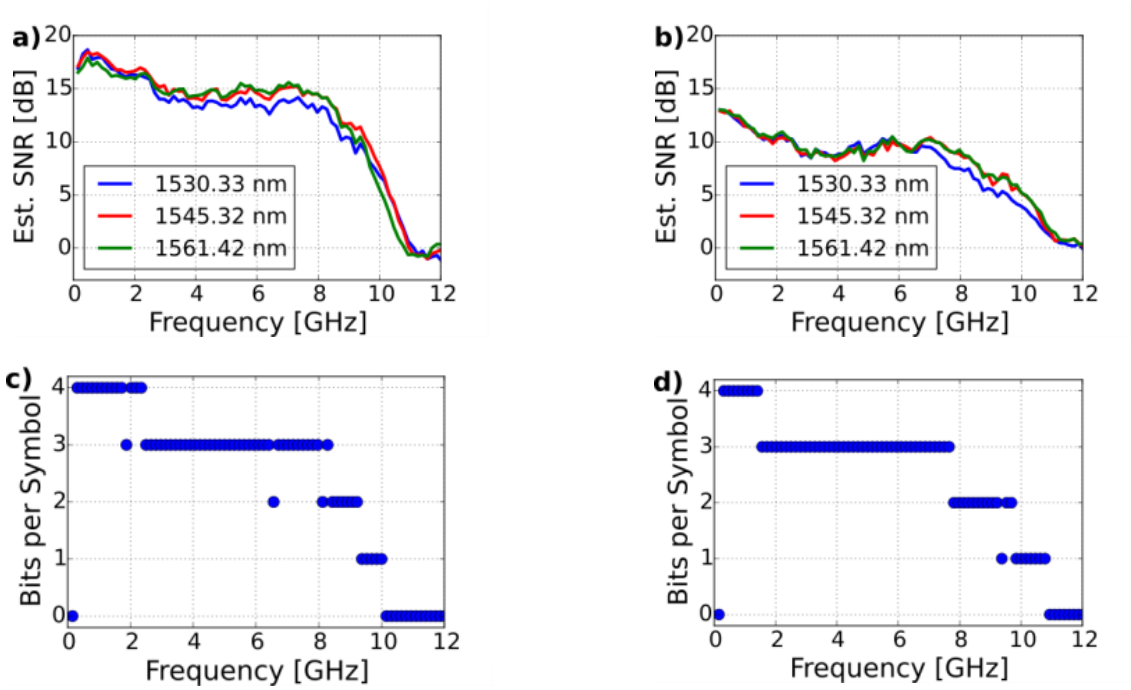

Figure 20: (a) Estimated SNR after 0 km SSMF for 3 measured wavelengths. (b) Estimated SNR after 40 km SSMF for 3 measured wavelengths. (c) Bit loading for 1530 nm wavelength after 0 km SSMF. (d) Bit loading for 1530 nm wavelength after 40 km SSMF.

We also tested the most typical transmission reaches. 20 km is the upper boundary for the fronthaul CPRI transmission, while 40 km is a typical reach for fixed enterprise access. The transmission results are shown in Figure 21.

The FEC limit is attained for all tested wavelengths and transmission reaches. The notable fact is the wavelength dependency. The performance at 1561.41 nm and 1545.32 nm is very similar for all tested transmission reaches. The similar error floors show that the laser chirp, laser nonlinearities, and residual dispersion are comparable for these wavelengths. The lower error floor at 20 km reach shows that the residual CD and the laser chirp optimally compensate for each other at this point. The slightly increased error floor in the back-to-back transmission compared to the strongly increased error floor at 40 km transmission shows that the system is more robust against negative CD.

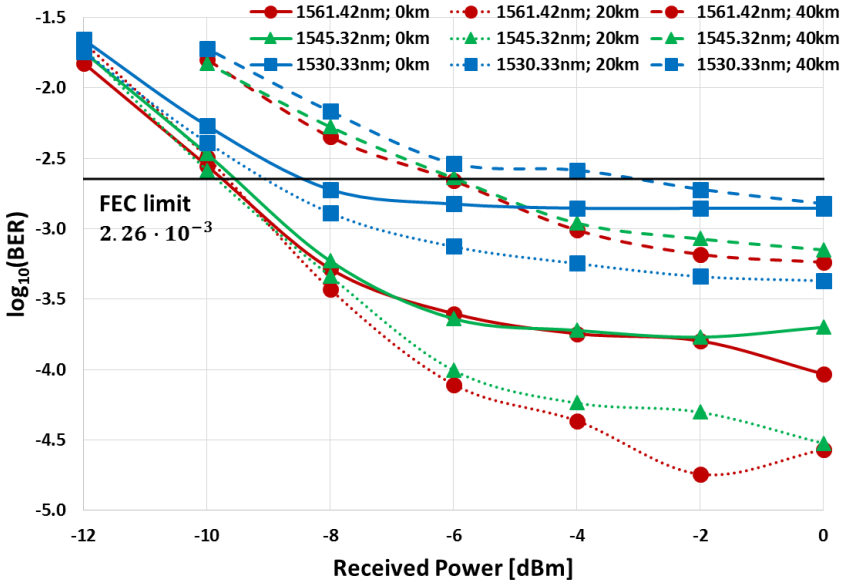

Figure 21: BER vs. received power at 26 Gbps for different wavelengths and transmission reaches.

In contrast to these two wavelengths, the shortest wavelength at 1530.33 nm shows an increased error floor. As described above, this wavelength is at the edge of the DBR mirror reflectivity leading to an increased laser threshold current and a reduced SNR. Furthermore, the linear region of the laser is reduced, while a linear transmitter is necessary for DMT to avoid subcarrier intermodulation products.

However, with the next generation of the MEMS-VCSEL we expect that the wavelength dependency over the whole C-band is removed. In the meantime, as elaborated in Section 3.1.4, half of the C-band can be used for the upstream and the other half for downstream. This reduces the wavelength dependency and helps to improve the reliability of the system.

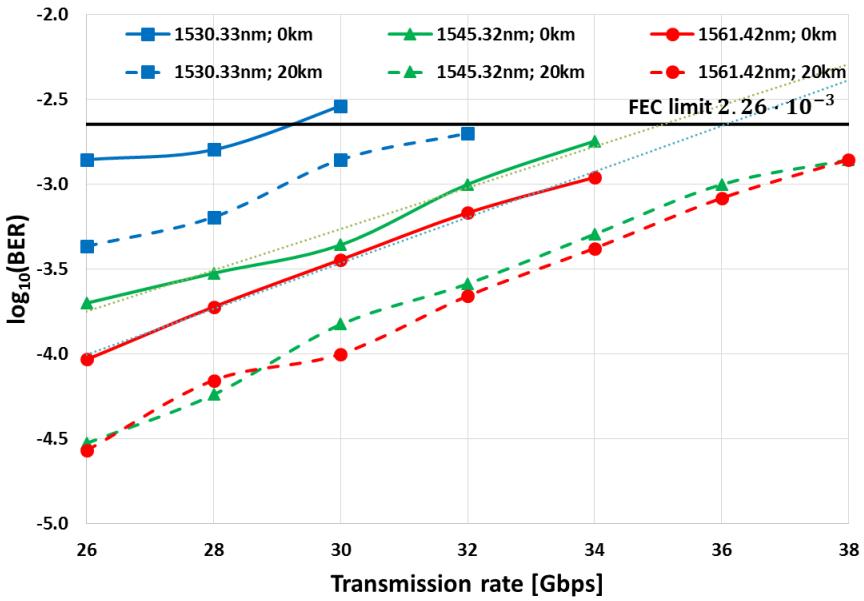

Figure 22: BER vs. transmission data rate for different wavelengths up to 20 km reach.

Figure 22 shows the performance versus the transmission data rate. Neglecting the 1530.33 nm wavelength, we demonstrate that the system is able to transmit bit rates beyond 35 Gbps on the longer wavelengths over 20 km transmission reach. This is even beyond CPRI option 10. Taking into account that CPRI is currently looking into other physical-layer splits (i.e. eCPRI) to reduce the necessary bit rate, this makes the proposed WDM-PON system with DMT modulation future-proof.

6. Conclusions

WDM-PON based on low-cost tuneable lasers as remote ONU transmitters has the potential to consolidate both front- and backhaul applications onto a common platform, thus lowering total network cost. This is enabled by the superior bit-rate × reach product of the laser transmitter per wavelength. To achieve economic feasibility, the cost of tuneable lasers needs to be reduced and new approaches are required. The cost reduction can be achieved by further relaxation of laser parameters, packaging and calibration requirements, and by the avoidance of componentry such as the TEC and a dedicated wavelength locker. Several tuneable laser technologies have been introduced, which could be able to meet these requirements. The resulting lasers then have to be controlled by a wavelength agnostic operation together with a centralized wavelength control.

We analysed the impairments in such a WDM-PON system using an AMCC in downstream direction for tracking the target wavelength of the ONU, and PTs in upstream direction were used as channel label. We also analysed the crosstalk caused by insufficiently calibrated lasers during the ONU start-up. The major challenge is high differential reach, but can be overcome by reducing the laser emitted power during tuning.

Finally, we demonstrated a 26 Gbps DMT transmission over 40 km SSMF using a tuneable MEMS-VCSEL with a tuning range of more than 30 nm. Discrete multitone modulation based on multiple subcarriers induced little expected impairments when the pilot tone and the second subcarrier had a large frequency deviation. This is suitable for the proposed WDM-PON system, and extends the system application to converged mobile and enterprise access with differential reaches of up to 40 km. For the fronthaul up to 20 km, we demonstrated future-proof transmission even beyond 35 Gbps.

In conclusion, WDM-PON systems based on low-cost tuneable lasers and centralized wavelength locking are therefore promising candidates for integrated mobile fronthaul, backhaul, and business access systems.

7. References

[1] K. Miyamoto, S. Kuwano, J. Terada, and A. Otaka, “Analysis of mobile fronthaul bandwidth and wireless transmission performance in split-PHY processing architecture,” Opt. Express, vol. 24, no. 2, pp. 1261–1268, 2016.

[2] 5G PPP, “View on 5G Architecture,” White Paper, July 2016. [Online] Available: https://5g-ppp.eu/white-papers/

[3] Gigabit-Capable Passive Optical Networks (GPON): General Characteristics, Amendment 2, Recommendation ITU-T G.984.1, 2012.

[4] 40-Gigabit-Capable Passive Optical Networks 2 (NG-PON2): Physical Media Dependent (PMD) Layer Specification, ITU-T G.989.2, 2014.

[5] 40-Gigabit-Capable Passive Optical Networks (NG-PON2): General Requirements, ITU-T G.989.1, 2013

[6] K. Grobe, M. H. Eiselt, S. Pachnicke, and J.-P. Elbers, “Access networks based on tunable lasers,” J. Lightw. Technol., vol. 32, no. 16, pp. 2815–2823, Aug. 2014.

[7] F. Ponzini et al., “Evolution Scenario Toward WDM-PON [Invited],” IEEE/OSA J. Opt. Commun. Netw., vol. 1, no. 4, pp. 25–34, Sep. 2009.

[8] Y. Luo et al., “Physical layer aspects of NG-PON2 standards—Part 2: System design and technology feasibility [Invited],” IEEE/OSA J. Opt. Commun. Netw., vol. 8, no. 1, pp. 43–52, Jan. 2016.

[9] H2020 Project 5G-XHaul, Deliverable D2.2 “System Architecture Definition,” [Online] Available: https://www.5g-xhaul-project.eu/

[10] S. Pachnicke et al., “Field demonstration of a tunableWDM-PON system with novel SFP+ modules and centralized wavelength control,” in Proc. Opt. Fiber Commun. Conf. Exhib., 2015, vol. 3, pp. 1–3.

[11] J. Zhu et al., “First demonstration of a WDM-PON system using full C-band tunable SFP+ transceiver modules [Invited],” IEEE/OSA J. Opt. Commun. Netw., vol. 7, no. 1, pp. A28–A36, Jan. 2015.

[12] S. H. Lee et al., “Athermal Colourless C-band Optical Transmitter for Passive Optical Networks,” in Proc. ECOC, Torino, 2010, Mo.1.B.2.

[13] K. Prince et al., “GigaWaM—next-generation WDM-PON enabling gigabit per-user data bandwidth,” J. Lightw. Technol., vol. 30, no. 10, pp. 1444–1454, May 2012.

[14] M. Iglesias, R. Rodes, T. T. Pham, and I. T. Monroy, “Real time algorithm temperature compensation in tunable laser/VCSEL based WDM-PON system,” in Proc. Int. Congr. UltraMod. Telecommun. Control Syst., 2012, pp. 240–242.

[15] S. Pachnicke, M. Roppelt, M. Eiselt, A. Magee, P. Turnbull, and J.-P. Elbers, “Investigation of wavelength control methods for next generation passive optical access networks,” in Proc. 38th Eur. Conf. Exhib. Opt. Commun., 2012, P6.02.

[16] J. Zhu et al., “High temperature athermal colorless transmitter for low-cost backhaul networks,” presented at the Conf. Lasers Electro-Optics, San Jose, CA, USA, Jun. 2014.

[17] Y. Rao, “InP-based long wavelength VCSEL using high contrast grating,” Ph.D. dissertation, EECS Dept., Univ. Calif., Berkeley, CA, USA, 2012.

[18] C. Gierl et al., “Tunable MEMS-VCSEL with >140-nm tuning range using SiO2/SiC-based MEMS-DBR,” in Proc. SPIE, Vertical-Cavity Surface-Emitting Lasers, vol. 9001, pp. 900107–1–900107-8, Feb. 2014.

[19] J. O. Wesström et al., “State-of-the-art performance of widely tunable modulated grating Y-branch lasers,” in Proc. OFC, Los Angeles, 2004, TuE2.

[20] D. C. J. Reid et al., “A novel broadband DBR laser for DWDM networks with simplified quasidigital wavelength selection,” in Proc. OFC, Anaheim, 2002, ThV5.

[21] T. Gruendl et al., “First 102 nm Ultra-Widely Tunable MEMS VCSEL Based on InP,” in Proc. IEEE Phot. Soc. 24th Ann. Mtg., 2011, ThDD1.

[22] Y. Rao et al., “Long-Wavelength VCSEL Using High-Contrast Grating,” J. Sel. Top. Quant. Electron., Vol. 19, no. 4, pp. 1701311, 2013.

[23] S. Paul et al., “Ultra wide mode-hop free tuning around 1550 nm telecom wavelength using high-speed MEMS-VCSELs,” J3, 20th Microoptics Conference, Fukuoka, 2015.

[24] S. Paul et al., “High speed surface micromachined MEMS tunable VCSEL for telecom wavelengths,” in Proc. CLEO, San Jose, 2015, AM3K.1.

[25] C. Wagner et al., “Full C-band Tunable MEMS-VCSEL for Next Generation G.metro Mobile Front- and Backhauling,” in Proc. OFC, Los Angeles, 2017, W2A27.

[26] K. Kondepu et al., “ Performance Evaluation of Next-Generation Elastic Backhaul with Flexible VCSEL-based WDM Fronthaul,” in Proc. ECOC, Gothenburg, 2017, W.1.E.4.

[27] C. Chase. et. al, “Tunable 1550nm VCSELs using high-contrast grating for next-generation networks,” in Proc. SPIE 9008, Optical Metro Networks and Short-Haul Systems VI, 900807, 2014.

[28] Z. Zhang et al., “C/L-Band Colorless ONU Based on Polymer Bidirectional Optical Subassembly,” J. Lightw. Technol., Vol. 33, no. 6, pp. 1230-1234, 2015.

[29] Common Public Radio Interface, “eCPRI 1.0 Specification,” August 2017. [Online] Available: http://www.cpri.info/.

[30] C. Wagner et al., “Impairment Analysis of WDM-PON based on Low-Cost Tunable Lasers,” J. Light. Technol., vol. 34, no. 22, 2016, pp. 5300-5307.

[31] John M. Cioffi, “Data Transmission Theory,” course text for EE379C. [Online] Available: http://www.stanford.edu/group/cioffi/.

[32] ITU-T Recommendation G.975.1, “Forward error correction for high bit-rate DWDM submarine systems – Appendix I.4,” 2004.

8. Acronyms

Acronym	Description
ADC	Analogue-to-Digital Converter
ADVA	ADVA Optical Networking SE
AMCC	Auxiliary Management and Communications Channel
AWG	Arrayed Waveguide Grating
BBU	Base Band Unit
BER	Bit-error Rate
BL	Bit Loading
BPSK	Binary Phase-Shift Keying
BTJ	Buried Tunnel Junction
C-RAN	Cloud Radio Access Network
CAPEX	CAPital EXpenditures
CD	Chromatic Dispersion
CO	Central Office
CoMP	Coordinated Multipoint
CP	Cyclic Prefix
CPRI	Common Public Radio Interface
CW	Continuous Wave
CWDM	Coarse WDM
DAC	Digital-to-Analogue Converter
DBR	Distributed Bragg Reflection
DCF	Dispersion Compensating Fibre
DMT	Discrete Multitone
DPL	Differential Path Loss
DS-DBR	Digital Supermode DBR Laser
DWDM	Dense WDM
eCPRI	Enhanced Common Public Radio Interface
EDFA	Erbium-Doped Fibre Amplifier
FEC	Forward Error Correction
FFR	Fractional Frequency Reuse
GbE	Gigabit Ethernet
Gbps	Gigabit per second
GCSR	Grating-assisted co-directional coupler laser with sampled grating reflector
IEEE	Institute of Electrical and Electronics Engineers
(I)FFT	(Inverse) Fast Fourier Transform

InP	Indium Phosphide
ITU-T	International Telecommunication Union-Telecommunication
LTE	Long Term Evolution
MEMS-VCSEL	Micro-Electromechanical System Vertical Cavity Surface Emitting Laser
mm-Wave	Millimetre-Wave
MZM	Mach-Zehnder Modulator
NRZ	Non-Return-to-Zero
ODN	Optical Distribution Network
OLT	Optical Line Terminal
ONU	Optical Network Unit
OPEX	OPerational EXpenditures
OTN	Optical Transport Network
P2P	Point-to-Point
PAM-4	Pulse Amplitude Modulation with four levels
PC	Polarization Controller
PIC	Photonic Integrated Circuit
PL	Power Loading
PON	Passive Optical Network
PRBS	Pseudo-Random Bit Sequence
PT	Pilot Tone
Q6/SG15	ITU-T Study Group 15, Question 6
QAM	Quadrature Amplitude Modulation
RAN	Radio Access Network
RAT	Radio Access Technology
RN	Remote Node
RRH	Remote Radio Head
SFP	Small Form-factor Pluggable
SFW	Single Fibre Working
SG-DBR	Sampled Grating DBR Laser
SIR	Signal-to-Interferer Ratio
SNR	Signal-to-Noise Ratio
SSMF	Standard Single Mode Fibre
TDMA	Time-Division Multiple Access
TEC	Thermo-electric Cooler
TIA	Trans-impedance Amplifier
TOSA	Transmitter Optical Subassembly
TS	Training Symbol

VOA	Variable Optical Attenuator
WDM	Wavelength Division Multiplexing
XGM	Cross Gain Modulation